Topological properties of singular fingers in frustrated cholesteric liquid crystals

J. Baudry, S. Pirkl,* and P. Oswald†
École Normale Supérieure de Lyon, Laboratoire de Physique,‡ 46 Allée d'Italie, 69364 Lyon Cedex 07, France
(Received 24 July 1997)

We study the nucleation of cholesteric fingers in directional growth when a cholesteric phase of positive dielectric anisotropy grows into its isotropic liquid. The experiment is performed in homeotropic anchoring and in electric field near the coexistence line of unwinding of the cholesteric helix. Four types of fingers can nucleate from the front: the normal (CF-1) and the spiraling fingers (CF-2), which are already known and the thin (CF-3) and thick fingers (CF-4), which had not been observed yet. From these observations and by solving numerically the Landau–Ginzburg–de Gennes equations for the director field, we propose a topological model for each finger. [S1063-651X(98)04603-0]

PACS number(s): 61.30.Gd, 61.30.Jf, 47.20.Ky

I. INTRODUCTION

In recent years, frustrated cholesteric liquid crystals of positive dielectric anisotropy attracted attention because of their ability to form various patterns in dc or ac electric field. Frustration and electric field can be simultaneously imposed by sandwiching the sample between two parallel electrodes coated with a silane that anchors the molecules perpendicularly to the surfaces. This homeotropic anchoring, which tends to align the molecules, is at the origin of the frustration: Indeed, the helical structure of the cholesteric phase cannot match with these boundary conditions. The electric field acts in the same manner [1], so that it becomes possible by increasing the electric field or by decreasing the sample thickness (or the confinement ratio $C=d/p$ of the sample thickness d over the equilibrium pitch p) to completely unwind the cholesteric phase and to obtain a homeotropic nematic phase. In practice, this cholesteric-nematic transition is first order (by using the language of the phase transitions) [2,3] so that there exists in the parameter plane (V,C) a coexistence line $V_2(C)$ where the two phases have exactly the same elastic energy and coexist. Nearby this line, elongated birefringent structures may form, which are called *cholesteric fingers*. Today, we know that two types of fingers exist at the very least. They closely resemble each other through the microscope, but their dynamical behaviors in an electric field are different [4–7].

In this article, we fully describe the topological and dynamical properties of isolated fingers and we show that two other types of fingers exist, which easily nucleate at a moving cholesteric-isotropic front. Our goal in this article is, first, to show how to distinguish the fingers of the different species, and, second, to give new information about their topological and energetical properties. In this respect, we have written a numerical algorithm similar to that proposed by Gil [8], which enables us to minimize the energy of a finger of a given topology in anisotropic elasticity.

The plan of the article is the following. In Sec. II, we describe the experimental setup and the way to make new fingers in directional solidification. In Secs. III–VI, we successively describe the fingers of the first to the fourth species. Section VII is devoted to their associations and to the possible connections they can form together. Finally, we propose in Sec. VIII new models for the director fields inside fingers.

II. EXPERIMENTAL SETUP AND PRELIMINARY OBSERVATIONS

In order to make fingers, we worked in directional solidification. This method has been extensively used to study interface pattern formation in alloys, plastic crystals, and liquid crystals [9]. Our apparatus was described in detail in Ref. [10] to which we refer for all technical information. In this experiment, the sample straddles the space between two ovens whose temperatures are individually controlled. The sample consists of two conducting glass plates (20×30 mm^2) recovered with ITO, which are separated by wire spacers, with a typical thickness of 20 μm. A mixture of 8CB (4-n-octylcyanobiphenyl) and of 0.62% by weight of chiral molecules S811 (E. Merck Co.) was introduced into the thin gap by capillarity. The two electrodes were coated with the silane ZLI 2979 (E. Merck Co.) in order to obtain a strong homeotropic anchoring (molecules perpendicular to the surfaces). Once in place, the sample was observed by optical microscopy, without polarizers. The temperatures of the two ovens were chosen in order that the cholesteric-isotopic front sits in the gap between the two ovens. The temperature gradient was measured by constructing a dummy sample with a thermocouple and measuring the temperature at different points in the gap between the two ovens. In our experiments, $G=28\,^\circ$C/cm.

In order to measure the equilibrium pitch p of our cholesteric mixture, we used the conventional Cano wedge method. We found $p\approx15\,\mu$m near the isotropic-cholesteric phase transition at $T_c\approx40\,^\circ$C. We also measured at this temperature the coexistence thickness d_c below which the cholesteric helix completely unwinds in homeotropic anchoring. We

*Permanent address: University of Pardubice, FES, Department of Physics, 53009 Pardubice, Czech Republic.
†Electronic address: oswald@physique.ens-lyon.fr
‡Associé au CNRS, URA 1325.

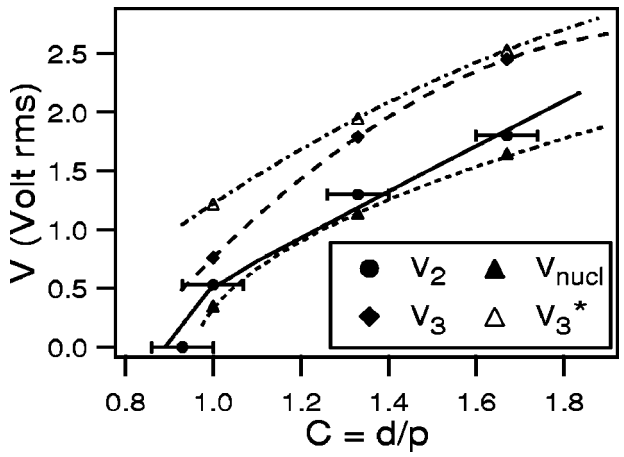

FIG. 1. Phase diagram at T_c. It only refers to the CF-1's that are nonsingular. Voltage $V_2(C)$ gives the coexistence line while $V_3(C)$ corresponds to the spinodal line of the CF-1's. Line V_{nucl} is the voltage below which CF-1's nucleate from the front at rest. The solid line has been calculated numerically without adjustable parameters.

found $d_c \approx 14\ \mu$m, which gives $C_c = d_c/p \approx 0.93$. The dimensionless parameter $C = d/p$ is called the confinement ratio. Finally, the homeotropic nematic phase becomes unstable (spinodal limit) when the confinement ratio is larger than $C_0 = d_0/p = K_{32}/2$ where $K_{32} = K_3/K_2$ is the ratio of the bend constant over the twist constant [2]. With the values of the elastic constants given in Ref. [11], we find $C_0 \approx 1$.

We used in our experiments of directional solidification three samples of thicknesses $d \approx 15$, 20, and 25 μm for which we calculate $C \approx 1$, 1.33, and 1.66 close to the phase transition temperature T_c. We thus expect the cholesteric phase is fully developed at the front in these three samples, which is indeed experimentally observed. In order to study the nucleation and the growth of isolated fingers at the front, we need to further unwind the cholesteric phase by applying an electric field ($f = 1$ kHz), and more precisely, a voltage close to the coexistence voltage $V_2(C)$ [2(a)]. We measured this voltage at T_c in the three samples as well as the voltage $V_3(C)$ above which the cholesteric phase become unstable (spinodal limit). Our results are reported in the phase diagram of Fig. 1. This phase diagram is established for cholesteric fingers of the first species (CF-1 in the following) which we know to be nonsingular.

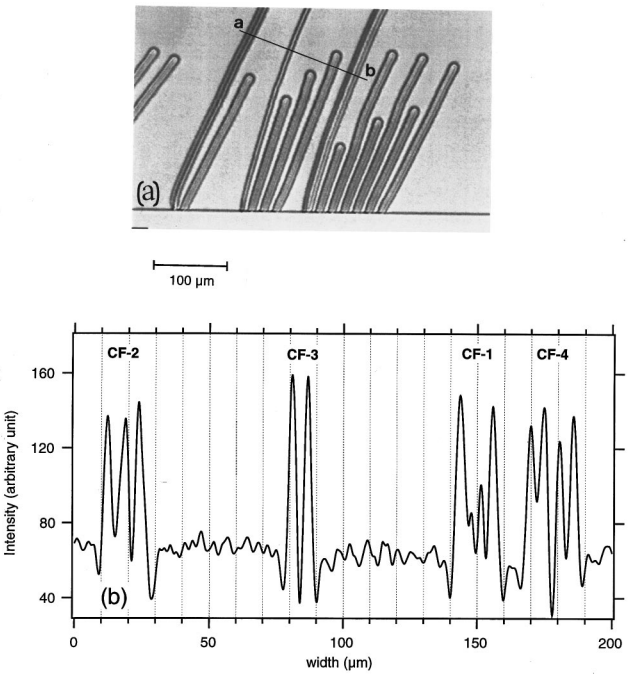

FIG. 2. (a) The four types of isolated fingers that can nucleate from the front with the isotropic liquid ($d = 20\ \mu$m, $V = 1.35$ V, $v = 4.3\ \mu$m/s); (b) intensity profile along a line a-b, which crosses the four types of fingers. The widths W_i of the different fingers are given in μm.

TABLE I. Relative width W_{i1} of a finger of the ith species with respect to a finger of the first species.

i	2	3	4
W_{i1}	1 ± 0.05	0.66 ± 0.04	1.29 ± 0.02

To conclude this section, let us briefly describe what happens in directional solidification at V_2 (or at a voltage that is slightly larger than V_2). At rest, the cholesteric phase is completely unwound and we only observe a nematic-isotropic front. When the pulling velocity is of a few μm/s, isolated fingers nucleate at the front. Usually, these fingers are CF-1's but it may happen that fingers of new types nucleate by pinning on dust particles crossing the interface. Sometimes these fingers unpin from the dust particles. In this case, they shorten and they can even collapse if the front velocity is too small. They can be of three types [Fig. 2(a)] with different optical contrasts as shown in Fig. 2(b) where we plotted their intensity profiles perpendicularly to their axes. Their apparent widths W_i, defined in Fig. 2(b), are also different. In the following, we shall call cholesteric fingers of the second species (CF-2) the fingers whose width W_2 is close to that of the CF-1's. We shall show in Sec. IV that they can give spirals in an ac electric field. By contrast, the cholesteric fingers of the third species (CF-3) are thinner than the CF-1's whereas the cholesteric fingers of the fourth species (CF-4) are thicker than the CF-1's. Finally, we have observed that the relative widths $W_{i1} = W_i/W_1$ of these ''abnormal'' fingers with respect to that of the CF-1's are roughly independent of the sample thickness within experimental errors. Values of W_{i1} are given in Table I.

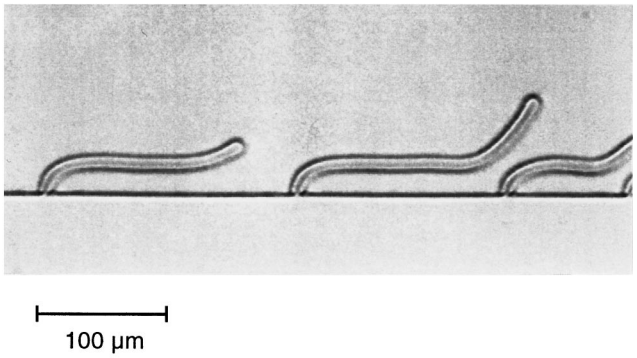

FIG. 3. Nucleation and growth of isolated CF-1's at the cholesteric-isotropic interface. $d = 20\ \mu$m, $V = 1.21$ V (intermediate between $V_2 = 1.28$ V and $V_{\mathrm{nucl}} = 1.14$ V), $v = 0\ \mu$m/s.

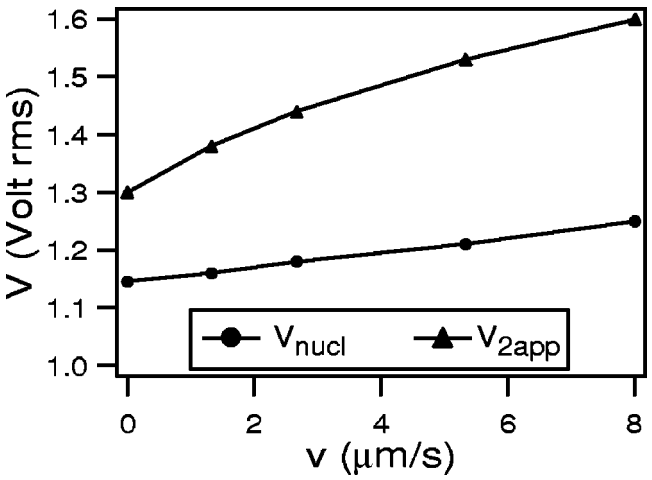

FIG. 4. Nucleation voltage V_{nucl} and apparent coexistence voltage $V_{2\,\mathrm{app}}$ of the CF-1's at the front as a function of the pulling velocity.

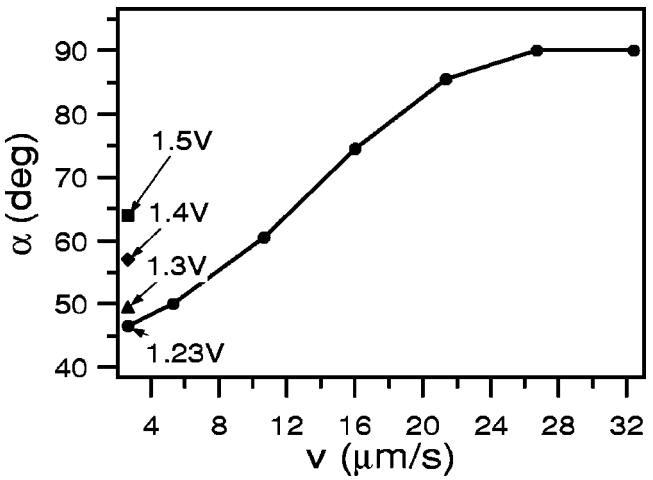

FIG. 6. Tilt angle α vs pulling velocity at a constant voltage $V=1.23$ V. We also reported a few values of α measured at constant velocity $v=2.67$ μm/s for different voltages.

In the following sections, we sum up the essential properties of the fingers of the different species.

III. FINGERS OF THE FIRST SPECIES (CF-1)

The CF-1's were known for a long time [12,2]. We recall that the director field inside a CF-1 is continuous as first shown by Press and Arrott [12(c)] and confirmed later by many authors [1,2,12]. These fingers grow spontaneously from the nematic-isotropic interface when the voltage is decreased below a well defined voltage V_{nucl} (Fig. 3). This voltage is slightly smaller than V_2 and slowly decreases when the pulling velocity increases (Fig. 4). It should be noted that the free end of each finger is always a rounded tip, which is energetically the more favorable [12(e),3(a)]. We also measured the apparent voltage $V_{2\ \mathrm{app}}$ for which the CF-1's do not grow in the field of the microscope. Because the sample is moving at velocity v, this voltage is also that for which the fingers shorten with velocity v. This easily explains why $V_{2\,\mathrm{app}}$ increases as a function of v. It is also possible to unpin these fingers from the interface by imposing a voltage close to V_3 during a very short time. At this voltage the CF-1's spontaneously break in many places, leading to short segments of a CF-1. These segments have already been described [12(e),2(a)] and are characterized by two different tips, which are called the normal and the abnormal tips (for instance, see Fig. 4(b) of Ref. [2(a)]). The normal tip is rounded and has everywhere the good twist whereas there is a small region in the abnormal tip where the twist does not have the right sign, which could explain why it is pointed. If the voltage is maintained above V_2, the segment of a CF-1 shortens and collapses. It was already shown

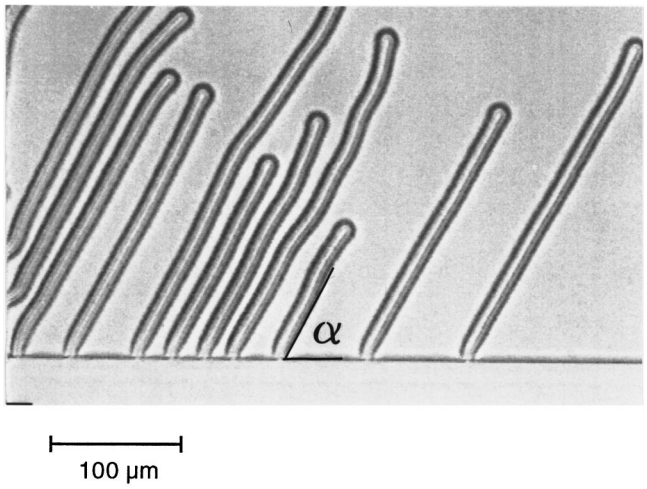

FIG. 5. Isolated cholesteric fingers observed at nonzero pulling velocity. They all make an angle α with the interface. $d=20$ μm, $V=1.23$ V, $v=10.7$ μm/s.

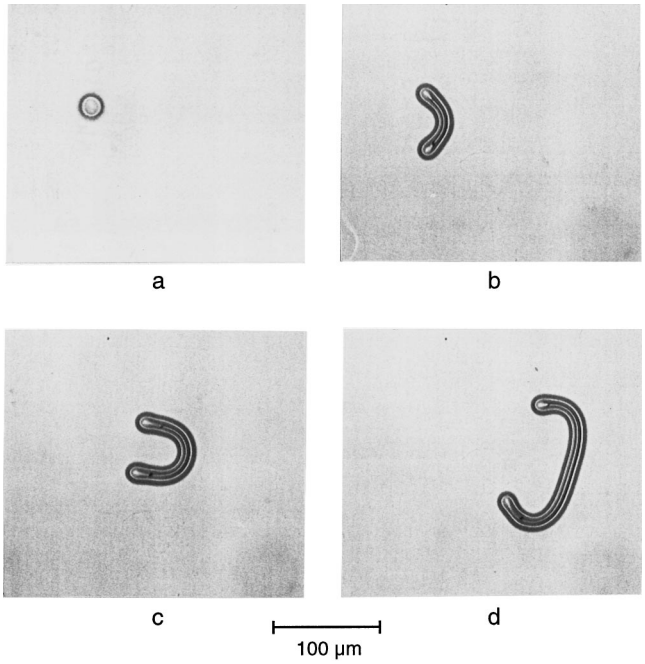

FIG. 7. Evolution in time of a CF-2 segment and formation of a spiral in an ac electric field ($d=25$ μm, $V=1.95$ V, $f=2$ kHz). This segment was obtained from the spherulite shown in (a) by temporarily decreasing the voltage below V_2. The time interval between two photographs is 5 ms.

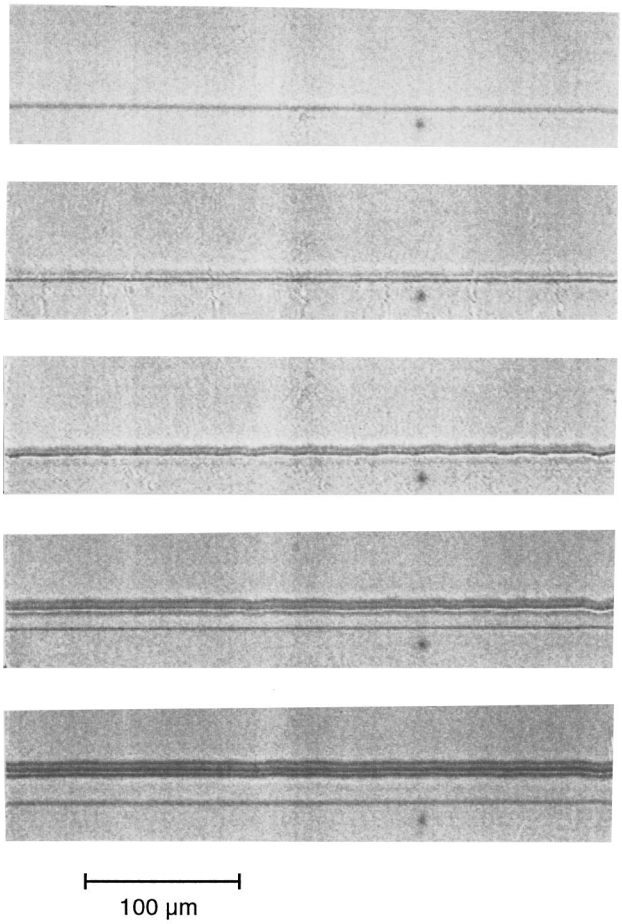

FIG. 8. Unpinning parallel to the front of a CF-2. $d=20\ \mu$m, $V=1.2$ V, $v=53.4\ \mu$m/s. The time interval between two photographs is 0.4 s.

that a segment of a CF-1 may slowly crawl along its axis at V_2 in an ac electric field of small enough frequency [6]. Finally, we have observed that the isolated fingers always make a well-defined angle α with the interface (Fig. 5), which depends on the pulling velocity and on the applied voltage (Fig. 6). This angle tends to $\pi/2$ (fingers perpendicular to the front) at large velocity and (or) large voltage.

IV. FINGERS OF THE SECOND SPECIES (CF-2)

The CF-2's are strongly connected with the cholesteric bubbles and give spirals in an ac electric field [6,7]. The

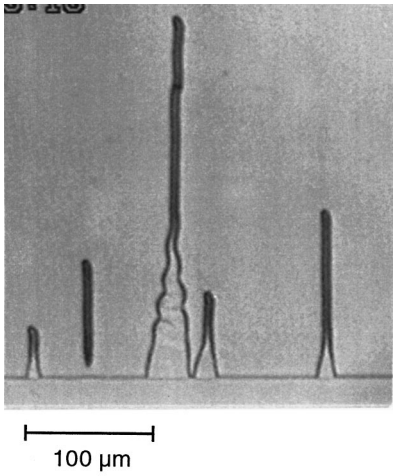

FIG. 9. Splitting of the foot of a thin finger of the third species into a triangle filled with a planar region ($d=15\ \mu$m, $V=1$ V, $v=40\ \mu$m/s).

cholesteric spirals were first observed by Gilli and Kamayé [4] in a polymeric liquid crystal and then by Mitov and Sixou [5] and ourselves [6,7] in ordinary liquid crystals. An already known property is that the two tips of a CF-2 segment look similar through the microscope and that such a segment shortens symmetrically at large voltage until a cholesteric bubble is formed (on the condition that the applied voltage is smaller than V_3^* corresponding to the spinodal limit of the bubbles; see Fig. 1). Recently, we also showed that a segment of a CF-2 can be made by stretching a cholesteric bubble at a voltage slightly smaller than V_2 [7]. We only succeed in reproducing this operation in the 25-μm-thick sample (Fig. 7). By contrast it is possible to make CF-2's in directional solidification. We have already mentioned in Sec. II that a CF-2 can form at small growth velocity when a dust particle crosses the nematic-isotropic interface. The CF-2 can then be unpinned from the dust particle and from the front by applying a large enough electric field. At large velocity, there exists another process of nucleation at the front of the CF-2's (Fig. 8). The sample is 20 μm thick and the velocity equals 53.4 μm/s. Under these conditions, and provided that the applied voltage is larger than $V_{\rm nucl}$ (in order that CF-1's do not nucleate) and not too large (i.e., a little bit smaller than V_2) fingers strictly parallel to the front detach from it at regular intervals of time. These fingers are very long but not infinite and are often attached to the front at their ends.

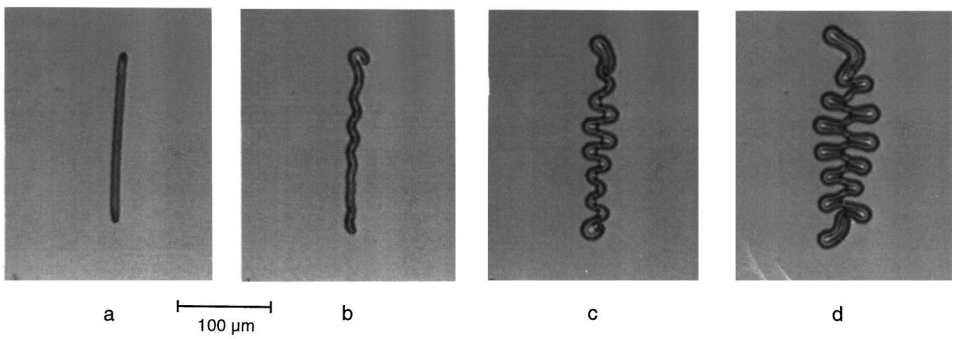

FIG. 10. Destabilization of a segment of a CF-3 when the voltage is decreased below V_2 ($d=25\ \mu$m, $V=1.8$ V) (a) $t=0$; (b) $t=6$ s; (c) $t=9$ s; (d) $t=12$ s.

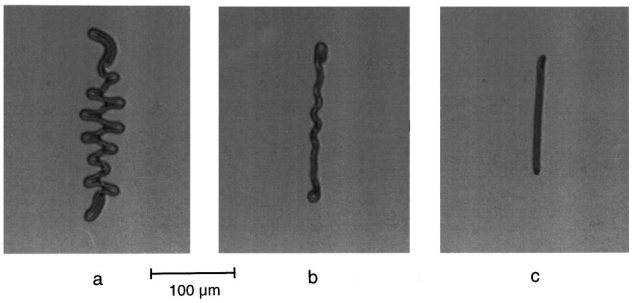

FIG. 11. The same finger as in Fig. 10(d) after increasing the voltage above V_2 ($d=25\ \mu$m, $V=2.2$ V). The CF-1's quickly disappear so that a segment of a CF-3 forms again. This segment then collapses. (a) $t=0$; (b) $t=3$ s; (c) $t=8$ s.

Again they can be unpinned from the front by temporarily increasing the voltage, which yields finite segments with similar ends. It is then possible to form a spiral from any such segment, which is the signature of a CF-2.

V. FINGERS OF THE THIRD SPECIES (CF-3)

The CF-3's are the thinnest of all (Table I). In contrast with the fingers of the first and of the second species, their nucleation always requires that a dust particle passes through the nematic-isotropic front. At small velocity, the CF-3's are well formed and have the same width until they join the front [Fig. 2(a)]. By contrast, their feet widen and split into triangles with ''planar'' regions inside, when the growth velocity increases. Such a phenomenon is shown in Fig. 9. These triangles have already been observed in the usual nematics in directional solidification and were considered to be due to the detachment by a dust particle of the disclination line that is pinned on the interface [13]. In usual nematics, the region within a triangle is in a planar orientation, i.e., with the molecules parallel to the glass plates in the middle of the sample. In cholesteric liquid crystals, this planar region may be unstable with respect to a periodic modulation parallel to the front. These observations clearly show that the CF-3's are singular and are obtained by associating two disclination lines. This problem will be discussed again in Sec. VII.

As for the CF-2's, it is possible to detach a CF-3 from the front and from the dust particle by temporarily increasing the voltage. In this way, a finite segment of a CF-3 with two similar free ends is obtained [Fig. 10(a)]. The later evolution of this segment strongly depends on the voltage. Either $V>V_2$ and the segment collapses (it never gives a cholesteric bubble in this case), or $V<V_2$ and the segment destabilizes as shown in Figs. 10(b) and 10(c). The destabilization starts by an undulation of the finger [Fig. 10(b)] followed by the growth of small segments of a CF-1 perpendicular to the finger axis. The two ends of the CF-3 are also unstable and curve (on the left or on the right) to form two ''hooks,'' which close up on themselves. This process leads to two segments of a CF-1 that are in the continuation of the CF-3. By increasing the voltage above V_2, the CF-1's disappear, first on the sides of the CF-3 and then at its ends if the finger is long enough. In this case, a segment of a CF-3 forms again to then collapse as before (Fig. 11). Sometimes, the portion of a CF-3 between the two CF-1's is very short and collapses

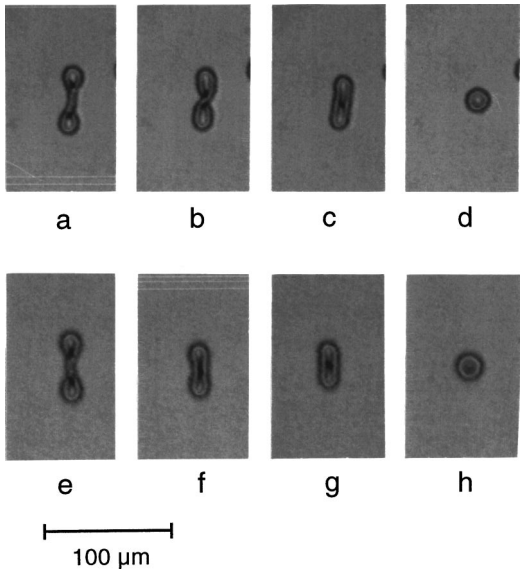

FIG. 12. Evolution of a short segment of a CF-3 with two CF-1's at its ends. In (a) the two ends are curved in opposite directions whereas in (e) they are curved in the same direction. $d=25\ \mu$m, $V=2.5$ V. For the first sequence we have (a) $t=0$, (b) $t=4$ s, (c) $t=7$ s, and (d) $t=18$ s while for the second one we have (e) $t=0$, (f), $t=3$ s, (g) $t=5$ s, and (h) $t=10$ s.

before the two CF-1's have completely disappeared. In this latter case, the finger no longer collapses and leads to a cholesteric bubble. Two possible sequences are shown in Fig. 12. In the sequence of Fig. 12(a), the two ends are curved in opposite directions whereas in Fig. 12(e), they are curved in the same direction. Nevertheless the final stage is a bubble in both cases.

In order to finish this section, we report that the CF-2's and the CF-3's can reversibly transform into each other de-

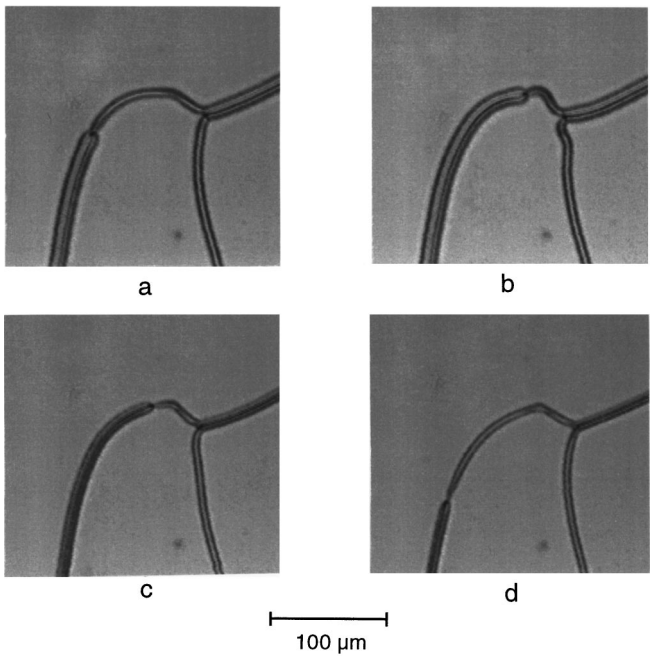

FIG. 13. (a), (b) Transformation of a CF-3 into a CF-2 at small voltage ($d=20\ \mu$m, $V=1.3$ V). (c), (d) The reverse transformation at large voltage ($d=20\ \mu$m, $V=1.8$ V).

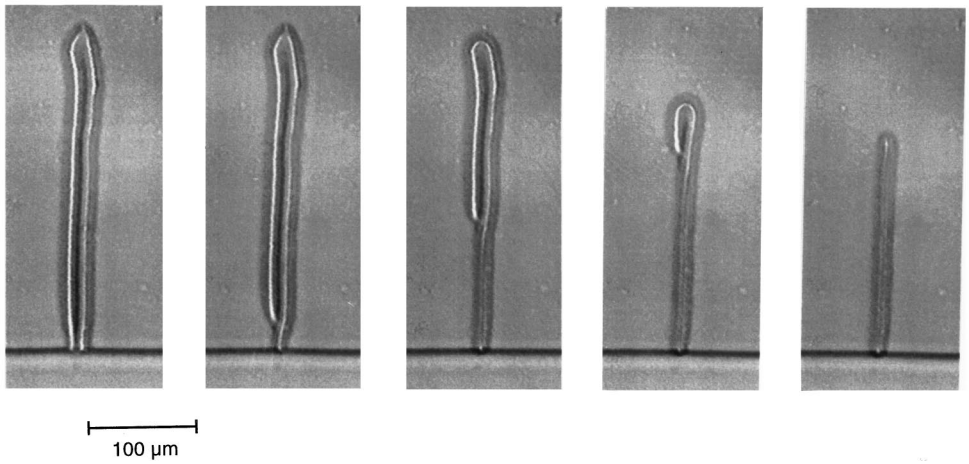

FIG. 14. Partial detachment of a CF-4 from the front leading to a portion of CF-3, which remains attached to the front. This transformation is irreversible.

pending on the voltage. This is shown in Fig. 13 where a CF-2 continues with a CF-3. The junction between the two fingers can move along their common axis depending on the applied voltage. Thus, the CF-2 is revealed to be more stable than the CF-3 at small voltage, whereas the CF-3 grows into the CF-2 at large voltage.

VI. FINGERS OF THE FOURTH SPECIES (CF-4)

The CF-4's are the thickest of all (Table I). They can be detached from the front by a dust particle. As opposed to the previous fingers, they can partly unpin from the front to give a thin finger that remains pinned on the front (Fig. 14). The thin finger being always more stable than the thick one, the thick fingers disappear very quickly. The larger the pulling velocity and the voltage, the faster they disappear. Note that we never obtained a finite segment of a CF-4 because of its spontaneous transformation into a CF-2, especially at large voltage. We also observed that below V_2, the CF-4 do not spontaneously branch on the sides with CF-1's as the CF-2's do, but just undulate a little bit (Fig. 15). Finally, the CF-4's can sometimes transform into a CF-2 (Fig. 16). This transformation is irreversible, the CF-4's being always energetically less favorable than the CF-2's.

VII. MULTIPLE CONNECTIONS BETWEEN FINGERS

We have seen in the previous sections that a finger of a given species can transform into a finger of another species, which enables us to compare the energies of the different fingers as a function of the thickness and of the applied voltage.

The fingers can also form more complicated connections. For instance, we very often observed T branchings of type (i,j), where a finger of the jth species connects on the side of a finger of the ith species [Fig. 17(a)]. Such connections are shown in Fig. 18 while we draw up in Table II all the cases we observed experimentally in our samples.

We also observed connections of type (i,j,k) [Fig. 17(b)] where three fingers of different species converge. Among the four possibilities, only (2,3,4) has been observed in the 20-μm-thick sample.

The next step is to find the topological structure of the different kinds of finger.

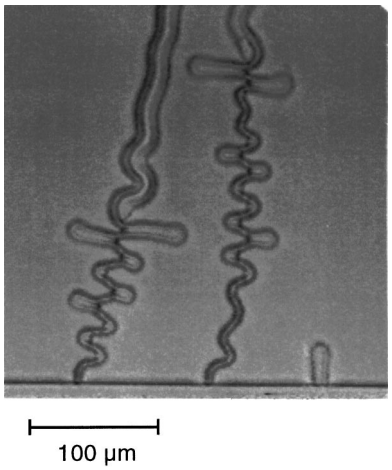

FIG. 15. Below V_2 the CF-3's are unstable and develop CF-1 sidebranching. By contrast the CF-4's only undulate a little bit ($d = 20\ \mu$m, $V = 1$ V, nematic-isotropic front at rest).

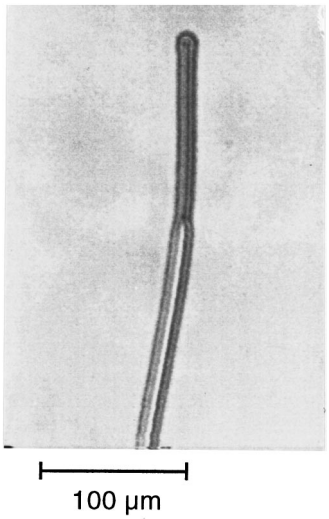

FIG. 16. Transformation of a CF-4 into a CF-2 ($d = 20\ \mu$m, $V = 1.8$ V).

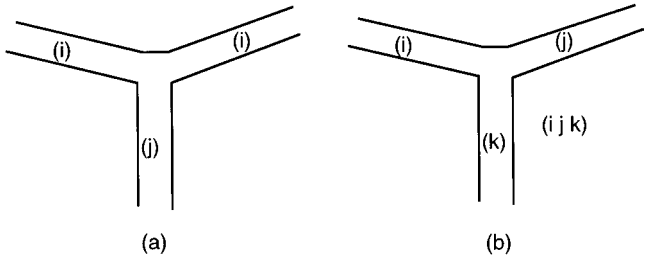

FIG. 17. Two types of multiple connection. In (a) two branches are identical whereas in (b) the three branches are different.

VIII. TOPOLOGICAL MODELS AND NUMERICAL SIMULATIONS

In order to characterize the fingers, we first looked for a topological model for each of them by using the previous experimental observations. Next, two-dimensional numerical simulations of the director field in a plane perpendicular to the finger axis for each type of finger were performed. Our simulation is a little different from that previously proposed by Gil [8]. The differences, as well as the limitations of the simulations, will be stressed later. These calculations consist in minimizing the elastic free energy for a given topology of the finger. Because of the presence of disclination lines of half integer rank in fingers of types 2, 3, and 4 (see below), we did all our calculations using the full Landau–Ginzburg–de Gennes expression for the elastic free energy density [14]:

$$f=\frac{1}{2}L_1\partial_i Q_{jk}\partial_i Q_{jk}+\frac{1}{2}L_2\partial_i Q_{ij}\partial_k Q_{kj}-\frac{1}{2}L_i q_0 \varepsilon_{ijk} Q_{il}\partial_k Q_{jl}+\frac{1}{2}AQ_{jk}Q_{kj}-\frac{1}{3}BQ_{jk}Q_{kl}Q_{lj}+\frac{1}{4}C(Q_{jk}Q_{kj})^2-\frac{1}{2}\mathbf{D}\cdot\mathbf{E}, \quad (1)$$

TABLE II. Possible T-branching connections i,j) [Fig. 17(a)]. In each case, the thickness of the sample in which we have observed the connection is given. This list is not exhuastive.

i \ j	1	2	3	4
1	Yes 10, 20, 25 μm	No	No	No
2	Yes 15 μm	Yes 20 μm	No	Yes 20 μm
3	Yes 15 μm	Yes 20 μm	Yes 20, 25 μm	Yes 25 μm
4	Yes 15 μm	Yes 20 μm	Yes 25 μm	Yes 20 μm

where $q_0=2\pi/p$ is the twist at equilibrium of the cholesteric phase. The tensor $Q=(Q_{ij})$ is the traceless, symmetric quadrupolar order parameter describing the local nematic order; it expresses in the uniaxial case as

$$Q_{ij}=\frac{Q}{2}(3n_i n_j-\delta_{ij}). \quad (2)$$

In this formula, Q is the amplitude of the order parameter and **n** the director, i.e., the unit vector parallel to the average direction of the molecules (it gives the isotropy axis of the tensor). In the simulations, we do not assume that Q_{ij} is uniaxial. Nevertheless, Q_{ij} is always found to be very close to a uniaxial tensor (except in the core of the disclination lines). In the following, we still call **n** the unit vector along the principal axis corresponding to the greatest eigenvalue of the Q_{ij} tensor (axis of quasi-isotropy of the tensor) and we shall simply represent the finger structure using the **n**-vector field.

Assuming the cholesteric phase is locally uniaxial, the electric field displacement **D** is related to the electric field **E** by the linear constitutive relation:

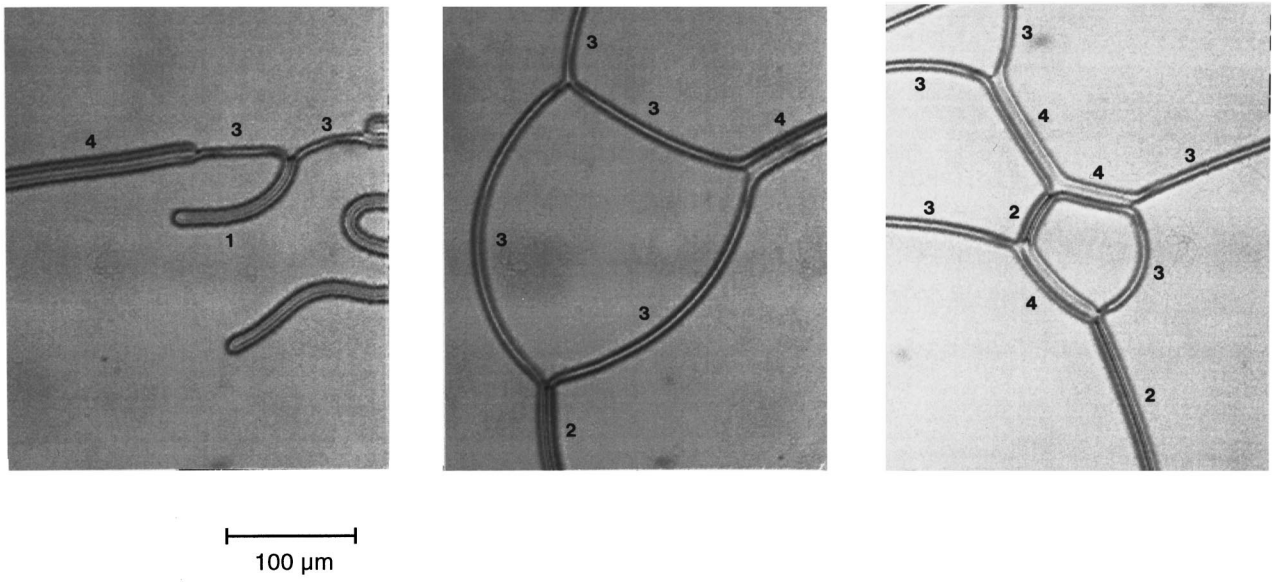

FIG. 18. Examples of possible connections between fingers of different species. The number beside each finger indicates of which species is the finger.

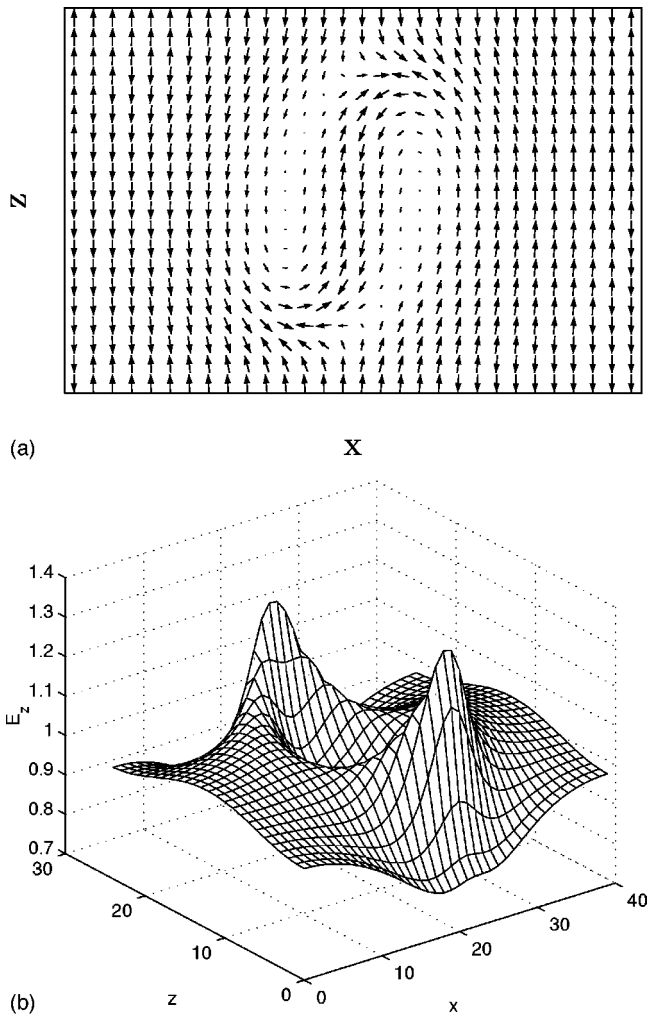

FIG. 19. (a) Director field inside a CF-1 calculated numerically at $C=1.33$ and $V=1.6$ V. The scale is the same on both axes; (b) vertical component of the electric field E_z in unit V/d calculated inside this finger.

$$\mathbf{D}=\underline{\varepsilon}\mathbf{E} \quad \text{with} \quad \underline{\varepsilon}=\varepsilon_{\text{iso}}\underline{\delta}+\varepsilon_a\underline{Q}, \tag{3a}$$

where

$$\varepsilon_{\text{iso}}=\frac{2\varepsilon_\perp+\varepsilon_\parallel}{3} \quad \text{and} \quad \varepsilon_a=\frac{2}{3}(\varepsilon_\parallel-\varepsilon_\perp). \tag{3b}$$

Note the multiplicative factor 2/3 in ε_a comes from the definition chosen (2) for the order parameter. Another assumption is that the frequency of the applied voltage is much larger than the charge relaxation frequency (dielectric regime).

In the uniaxial approximation, the elastic Frank constants are related to constants L_1 and L_2 via the relations

$$K_1=K_3=\frac{9}{4}(2L_1+L_2)Q^2, \tag{4a}$$

$$K_2=\frac{9}{2}L_1Q^2. \tag{4b}$$

Note that the splay and bend constants are equal in this model, which is observed near an isotropic-nematic phase transition. Relations (4a) and (4b) are useful to calculate L_1 and L_2 from the experimental values of the Frank constants measured in the nematic phase [11].

The equations to solve at equilibrium are obtained by minimizing Eq. (1) with respect to the electric potential U and the 5 independent coefficients $Q_{11},Q_{22},Q_{12},Q_{13},Q_{23}$:

$$-\frac{\delta f}{\delta Q_{ij}}=\frac{d}{dx_k}\frac{\partial f}{\partial Q_{ij,k}}-\frac{\partial f}{\partial Q_{ij}}=0, \tag{5a}$$

$$-\frac{\delta f}{\delta U}=\text{div}\,\mathbf{D}=0. \tag{5b}$$

In practice, we use a relaxation method and solve the following equations:

$$\frac{\partial Q_{ij}}{\partial t}=-\frac{\delta f}{\delta Q_{ij}}, \tag{6a}$$

$$\frac{\partial U}{\partial t}=-\frac{\delta f}{\delta U}. \tag{6b}$$

Boundary conditions on the two limiting surfaces are

$$Q_{12}=Q_{23}=Q_{13}=0 \quad \text{at} \quad z=0 \quad \text{and} \quad z=d, \tag{7a}$$

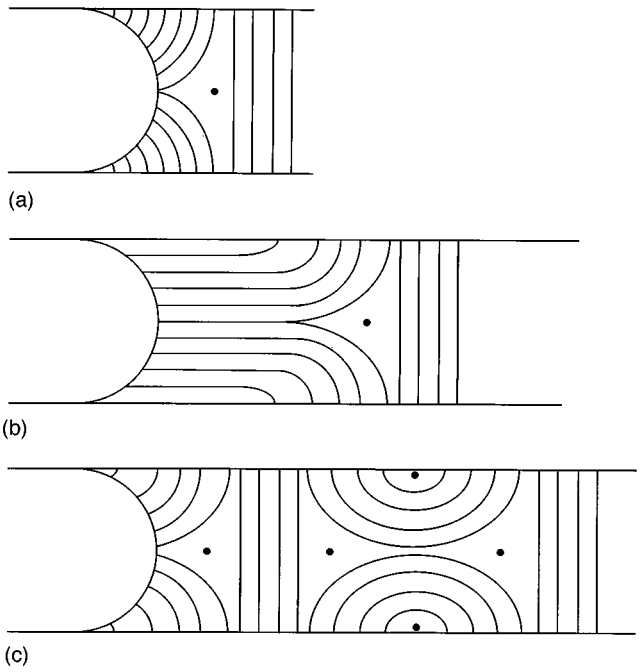

FIG. 20. Possible scenario for the formation of a CF-2 from the cholesteric-isotropic front. (a) For topological reasons, a $-1/2$ wedge disclination line lies on the front; (b) at large enough velocity, this line detaches, leading to a planar region; (c) this planar region is unstable and becomes homeotropic again. This process leads to a cholesteric finger containing four disclination lines (two $-1/2$ and two $+1/2$ in order that the global topological charge remains zero), while the $-1/2$ line forms again on the front.

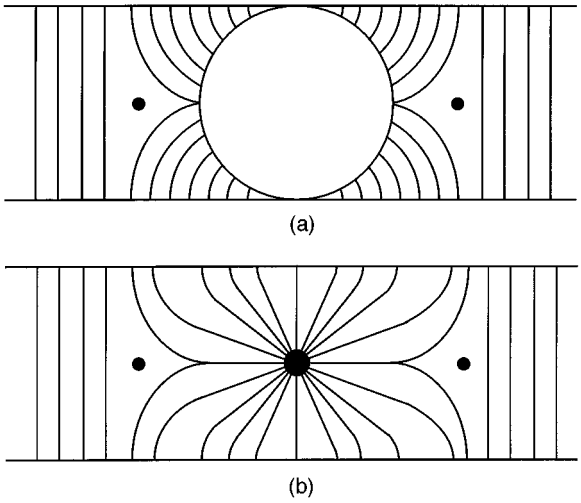

FIG. 21. Formation of a CF-2 from a bubble of isotropic liquid. (a) Two $-1/2$ disclination lines bordering a bubble of isotropic liquid with strong homeotropic anchoring; (b) Freezing the isotropic liquid leads to the formation of a $+1$ disclination line. This model is topologically equivalent to the model of Fig. 20.

$$Q_{11}=Q_{22}=-\frac{1}{2}\,Q_\infty \quad \text{at } z=0 \quad \text{and} \quad z=d, \tag{7b}$$

$$U=O \quad \text{at} \quad z=0, \tag{7c}$$

$$U=V \quad \text{at} \quad z=d, \tag{7d}$$

where V is the applied voltage and Q_∞ the value of the amplitude of the order parameter in the cholesteric phase at equilibrium. Note that we assume here that the phase is uniaxial and homeotropically oriented on the two limiting surfaces.

This numerical simulation is different from that previously proposed by Gil [8] in three respects: First, we do not assume that Q_{ij} is a uniaxial tensor of constant amplitude; by contrast, we calculate at each point its five independent components; second, we locally solve the electric field, which we know to be very inhomogeneous in such distorted structures [2(c)]; third, we used the same numerical algorithms as those proposed by Sonnet *et al.* [15] for calculating the core structure of disclination lines in nematic liquid crystals.

The problem now is to choose an initial configuration for each type of finger compatible with its real topology. This is crucial because most of them contain defects that never appear spontaneously in the two-dimensional simulations. The previous experimental results can be used for guiding us in the choice of the initial configurations. Let us start with the normal fingers or CF-1, which are nonsingular.

A. Normal finger or CF-1

The structure of these fingers is now very well known. They were first numerically calculated by Press and Arrott [12(c),(d)] in isotropic elasticity. More recently, topological models using a representation on the unit sphere $S2$ were proposed to calculate their structure in anisotropic elasticity [2,3]. This model was recently confirmed by numerical simulations of Gil [8] and of Nagaya *et al.* [16]. We did similar calculations, except that we further solve the local electric field. The starting configuration can be either the homeotropic nematic state (below its spinodal limit), or the director field given by the ''double-twisted'' model on $S2$ proposed in Refs. [2, 3]. Both lead to the same final configuration. An example is shown in Fig. 19(a). These simulations allowed us to determine the coexistence line $V_2(C)$ of the phase diagram. On this line, the two phases have exactly the same energy. This line is plotted in Fig. 1 and has been calculated by using numerical values of the elastic constants and of the dielectric constants given in the literature [11,17] ($K_1=K_3$, $K_1/K_2=2.1$, $K_2=1.5\times10^{-7}$ dyn, $\varepsilon_\parallel=13.7$, and $\varepsilon_\perp=6.2$). The temperature is chosen 2 °C below T_c and coincides with the spinodal temperature T^* of the isotropic liquid [18]. Thus, we set $A=0$ in our simulation. The other Landau constants are calculated using the values of the latent heat ($\Delta H\approx2.06$ J/cm^3 [19]) and of the first Landau coefficient [$A=A_0(T-T^*)$, $A_0\approx0.19$ J/cm^3/K [19]]. This procedure gives $B\approx4.3$ J/cm^3, $C\approx11$ J/cm^3, and $Q_\infty=B/C\approx0.4$ at T^*. By using Eq. (4) we also calculate $L_1=4.7\times10^{-7}$ dyn and $L_2/L_1=2.2$. With these values, the calculated coexistence line is in very good agreement with the experimental

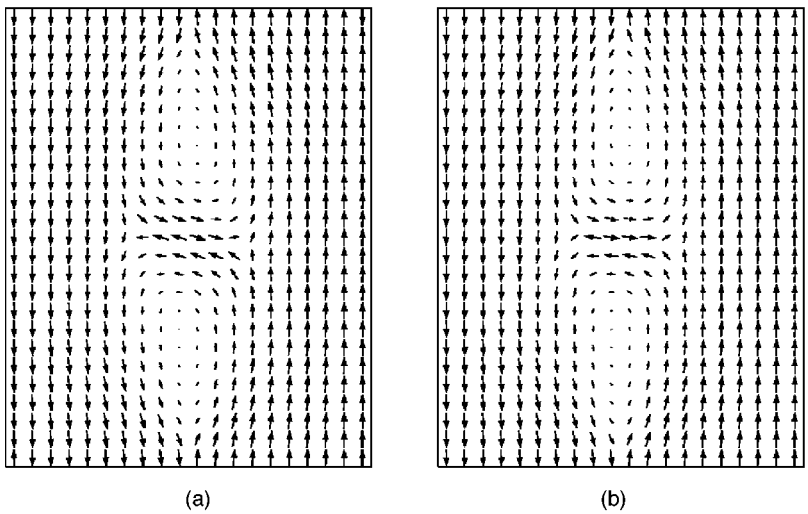

FIG. 22. CF-2 numerically obtained by starting from (a) the model of Fig. 20 and (b) the model of Fig. 21 ($C=1.33$, $V=1.6$ V).

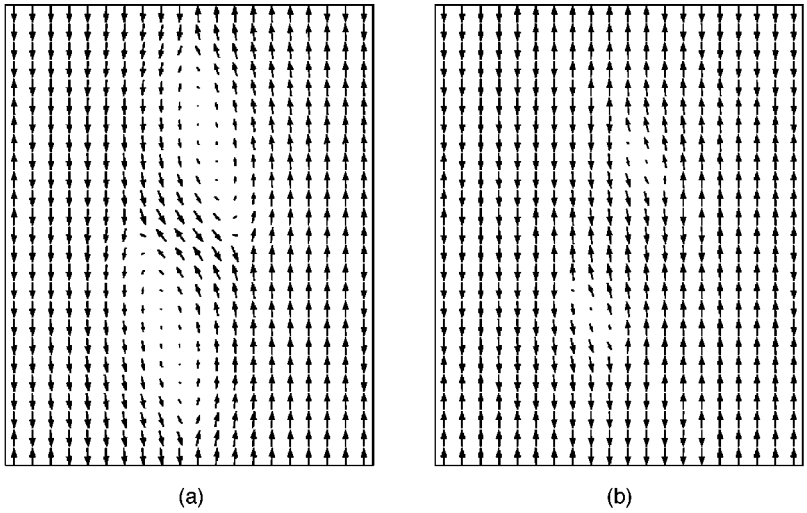

FIG. 23. Numerical evolution as a function of the applied voltage of a CF-2 at $C=1.33$. (a) $V=2.3$ V, (b) $V=4.3$ V.

curve. It should be noted that the calculations are done without adjustable parameters. In Fig. 19(b), we plotted the z component of the electric field across the finger: as expected the electric field varies by $\pm 30\%$ about its mean value V/d.

B. Spiralling finger or CF-2

The experiment shows that CF-2's can detach homogeneously from the cholesteric-isotropic front in directional growth at large enough velocity. We propose that this process is due to a detachment of the $-1/2$ wedge disclination line, which is pinned on the meniscus separating the two phases, immediately followed by the formation of an unstable planar region that destabilizes to give again a nematic band separated by two $-1/2$ disclinations. One of them is pinned on the interface whereas the other forms with the first one the CF-2. Note that for topological reasons, two 1/2 disclinations must nucleate in the same time nearby the glass plates. The resulting finger is thus composed by four disclination lines disposed as drawn in Fig. 20(c).

Another way to justify this model is to remember that the CF-2's are strongly connected with the cholesteric bubble [12(e),7]. Indeed, a CF-2 can be obtained by stretching a cholesteric bubble, which means that the bubble and CF-2 are topologically equivalent. We also recall that a cholesteric bubble can be obtained by freezing a droplet of isotropic liquid [20]. In this case, we obtain a $+1$ disclination line bordered by two $-1/2$ disclinations as shown in Fig. 21. This configuration is another possible starting point for the simulations.

It turns out that both initial configurations almost lead to the same final finger, as shown in Fig. 22.

The small difference between the two final configurations comes from a partial pinning of the disclination lines on the numerical grid. Indeed, there are two very different length scales in this problem: the cholesteric pitch (of the same order as the sample thickness) $p \approx 15\ \mu$m, and the core radius of the disclination lines of the order of $r_c \approx \sqrt{L/BQ_\infty} \approx 20$ Å. Consequently, a $10^4 \times 10^4$ grid would be necessary to numerically solve the problem at the two length scales, which is beyond the capacity of our computer. To bypass this difficulty, we used a smaller grid (typically 100×100) and we artificially increased the core size of the disclinations by

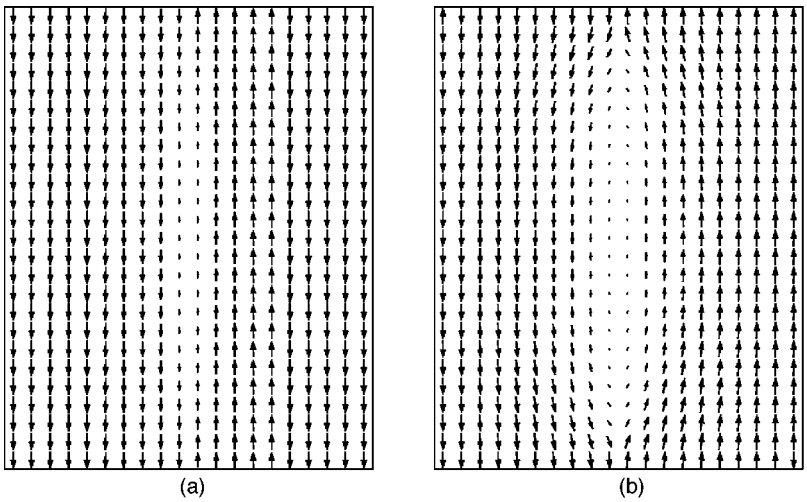

FIG. 24. Numerical simulation of a thin CF-3. (a) Starting configuration containing two twist disclination line of angles π and $-\pi$ located near to the glass plates; (b) obtained configuration at $C=1.33$ and $V=1.6$ V.

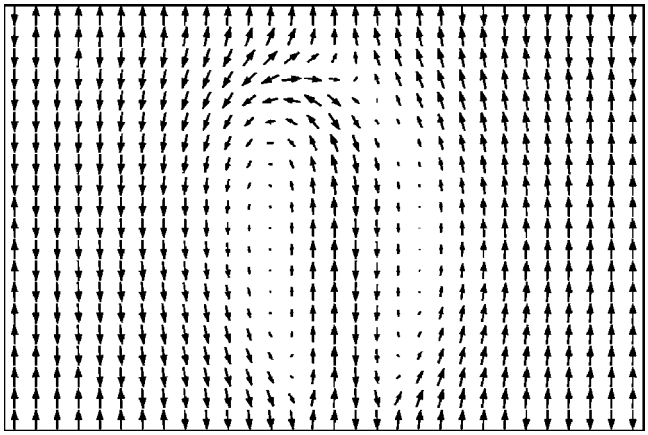

FIG. 25. Numerical simulation of a thick CF-4 finger ($C = 1.33$ and $V = 1.6$ V).

decreasing B and C by a constant multiplicative factor f, typically $f \approx 10\,000$. In this way, the core radius becomes comparable to the mesh size, which avoids a too strong pinning of the defects on the grid. In addition, the values of the elastic Frank constants remain unchanged as well as the value of Q_∞, so that the structure is correctly computed at large scale (larger than the mesh size). This method has nevertheless two drawbacks: First, the final configuration depends a little bit on the choice of the renormalization factor f, although the topology of the finger is always the same. This explains the difference between the two configurations shown in Fig. 22. Second, it forbids a precise calculation of the finger's energy; indeed, the elastic energy of each disclination line is underestimated by about $K_2 \ln(a/r_c) \approx 3K_2$, where a is the mesh size and r_c the core radius. This error is not negligible compared to the elastic energy of the whole configuration, typically $15K_2$. Thus, our calculation cannot be used to compare the energies of the different types of fingers.

Anyway, we propose that spiralling fingers are composed of four disclination lines as shown in Fig. 22. Their evolution as a function of the electric field is shown in Fig. 23. At large voltage, these fingers become very narrow, which is observed experimentally.

C. Thin finger or CF-3

This finger is about two times thinner than the others, which suggests that the director rotates by π rather than 2π across the finger in the middle plane. Another important observation is that the fingers form from the triangles, which detach from the nematic-isotropic front in directional solidification. More precisely, they nucleate when the two sides of the triangle join together. Thus, a thin finger is composed of two twist disclination lines of angles $+\pi$ and $-\pi$. Starting numerically from such an association [Fig. 24(a)], we obtain after relaxation the final configuration shown in Fig. 24(b). As expected the director rotates by π across the finger. This type of finger has already been proposed by Kléman and Cladis [21] and then numerically calculated by Gil [8]. Our contribution is to have clearly characterized this finger experimentally and to show that it does not drift perpendicularly to its axis in ac electric field and never gives spiral.

D. Thick finger or CF-4

We did not clearly observe how this finger nucleated, so attributing a special structure to this finger is difficult. The two main observations are that this finger is a little wider than CF-1 or CF-2 and transforms very easily into a CF-3. For this reason we propose the model described in Fig. 25: the finger is composed of two twist disclination lines of angle π localized close to one plate. This structure matches to the other plate via a half-normal finger. The simulations show that this finger is wider than the others, as observed experimentally, and transforms easily into a CF-3 when the electric field is increased. During this process one line moves to the opposite plate and changes sign.

IX. CONCLUSION

At least four types of cholesteric fingers have been characterized in confined geometry. One of them is topologically continuous (CF-1) whereas the others (CF-2,3,4) have four or two disclination lines along their axes. Their behaviors in ac electric field differ depending on their topology. We propose that only fingers containing four disclination lines drift perpendicularly to their axes and may form spirals.

It would be now very important to understand the origin of this drift. Preliminary measurements of the drift velocity of CF-2 show it strongly depends on the electric conductivity of the liquid crystal. Such measurements are now in progress and will be published in a forthcoming article.

ACKNOWLEDGMENTS

This work was supported by DRET Contract No. 95.1117 and by the European Research Network Contract No. FMRX-CT96-0085.

[1] (a) P. G. de Gennes, Solid State Commun. **6**, 163 (1968); (b) R. B. Meyer, Appl. Phys. Lett. **12**, 281 (1968); (c) **14**, 208 (1969); (d) G. Durand, L. Leger, F. Rondelez, and M. Veyssie, Phys. Rev. Lett. **22**, 227 (1969).

[2] (a) P. Ribière and P. Oswald, J. Phys. (France) **51**, 1703 (1990); (b) P. Ribière, S. Pirkl, and P. Oswald, Phys. Rev. A **44**, 8198 (1991); (c) P. Ribière, Thèse, Université Claude Bernard-Lyon I, No 289.92, Déroulage d'un Cholestérique Frustré en Champ Electrique (1992).

[3] F. Lequeux, J. Bechhoefer, and P. Oswald, Phys. Rev. A **40**, 3974 (1989).

[4] (a) J. M. Gilli and M. Kamayé, Liq. Cryst. **11**, 791 (1992); (b) **12**, 545 (1992).

[5] (a) M. Mitov and P. Sixou, J. Phys. II **2**, 1659 (1992); (b) Mol. Cryst. Liq. Cryst. **231**, 11 (1993); (c) Mod. Phys. Lett. B **9**, 929 (1995); (d) Physica B **216**, 132 (1995).

[6] P. Ribière, P. Oswald, and S. Pirkl, J. Phys. II **4**, 127 (1994).

[7] S. Pirkl and P. Oswald, J. Phys. II **6**, 355 (1996).

[8] L. Gil, J. Phys. II **5**, 1819 (1995).
[9] P. Oswald, J. Bechhoefer, and F. Melo, MRS Bull. **XVI**, 38 (1991).
[10] P. Oswald, M. Moulin, P. Metz, J. C. Géminard, P. Sotta, and L. Sallen, J. Phys. III **3**, 1891 (1993).
[11] N. V. Madhusudana and R. Pratibha, Mol. Cryst. Liq. Cryst. **89**, 249 (1982).
[12] (a) M. Brehm, H. Finkelmann and H. Stegemeyer, Ber. Bunsenges. Phys. Chem. **78**, 883 (1974); (b) T. Harvey, Mol. Cryst. Liq. Cryst. **34**, 224 (1978); (c) M. J. Press and A. S. Arrott, J. Phys. (France) **37**, 387 (1976); (d) Mol. Cryst. Liq. Cryst. **37**, 81 (1976); (e) A. J. Stieb J. Phys. (France) **41**, 961 (1980); (f) S. Pirkl, Cryst. Res. Technol. **26**, 371 (1991).
[13] P. Oswald, J. Bechhoefer, and A. Libchaber, Phys. Rev. Lett. **58**, 2318 (1987).
[14] P. G. de Gennes and J. Prost, *The Physics of Liquid Crystals* (Oxford University Press, Oxford, 1993).
[15] A. Sonnet, A. Kilian, and S. Hess, Phys. Rev. E **52**, 718 (1995).
[16] T. Nagaya, Y. Hikita, H. Orihara, and Y. Ishibashi, J. Phys. Soc. Jpn. **68**, 2713 (1996).
[17] B. R. Ratna and R. Shashidhar, Mol. Cryst. Liq. Cryst. **42**, 113 (1977).
[18] H. J. Coles and C. Stratielle, Mol. Cryst. Liq. Cryst. **55**, 273 (1979).
[19] H. Marynissen, J. Thoen, and W. Van Kael, Mol. Cryst. Liq. Cryst. **97**, 149 (1983).
[20] S. Pirkl, P. Ribière, and P. Oswald, Liq. Cryst. **13**, 413 (1993).
[21] P. E. Cladis and M. Kléman, Mol. Cryst. Liq. Cryst. **16**, 1 (1972).